Hydrophobicity attainment and wear resistance enhancement on glass substrates by atmospheric plasma-polymerization of mixtures of an aminosilane and a fluorocarbon

Rodolfo Múgica-Vidal [(a)], Fernando Alba-Elías [(a)], Elisa Sainz-García [(a)], Mariola Pantoja-Ruiz [(b)]

(a) Department of Mechanical Engineering. University of La Rioja. c/ Luis de Ulloa 20, 26004 Logroño, La Rioja, Spain.

(b) Materials Science and Engineering Department, IAAB, Materials Performance Group, University Carlos III of Madrid. Av. Universidad 30, 28911 Leganés, Madrid, Spain.

Accepted Version for publication in Applied Surface Science

Link to publisher version (DOI): https://doi.org/10.1016/J.APSUSC.2015.04.089

Published source citation:

Múgica-Vidal, R., Alba-Elías, F., Sainz-García, E., & Pantoja-Ruiz, M. (2015). Hydrophobicity attainment and wear resistance enhancement on glass substrates by atmospheric plasma-polymerization of mixtures of an aminosilane and a fluorocarbon. *Applied Surface Science*, *347*, 325-335. https://doi.org/10.1016/J.APSUSC.2015.04.089

Author names and affiliations:

Rodolfo Múgica-Vidal
Department of Mechanical Engineering
University of La Rioja
c/ Luis de Ulloa 20, 26004 - Logroño, La Rioja, Spain.
Tel.: +34 941299276; fax: +34 941299794.
E-mail address: rodolfo.mugica@alum.unirioja.es

Elisa Sainz-García
Department of Mechanical Engineering
University of La Rioja
c/ Luis de Ulloa 20, 26004 - Logroño, La Rioja, Spain.
Tel.: +34 941299276; fax: +34 941299794.
E-mail address: elisa.sainzg@unirioja.es

Mariola Pantoja-Ruiz
Materials Science and Engineering Department, IAAB, Materials Performance Group
University Carlos III of Madrid
Av. Universidad 30, 28911 - Leganés, Madrid, Spain.
Tel.: +34 916248863; fax: +34 916249440.
E-mail address: mpruiz@ing.uc3m.es

Corresponding author:

Fernando Alba-Elías
Department of Mechanical Engineering
University of La Rioja
c/ Luis de Ulloa, 20, 26004 - Logroño, La Rioja, Spain.
Tel.: +34 941299276; fax: +34 941299794.
E-mail address: fernando.alba@unirioja.es

ABSTRACT

Mixtures of different proportions of two liquid precursors were subjected to plasma-polymerization by a non-thermal atmospheric jet plasma system in a search for a coating that achieves a hydrophobic character on a glass substrate and enhances its wear resistance. 1-perfluorohexene (PFH) was chosen as a low-surface-energy precursor to promote a hydrophobic character. Aminopropyltriethoxysilane (APTES) was chosen for its contribution to the improvement of wear resistance by the formation of siloxane bonds. The objective of this work was to determine which of the precursors mixtures that were tested provides the coating with the most balanced enhancement of both hydrophobicity and wear resistance, given that coatings deposited with fluorocarbon-based precursors like PFH are usually low in resistance to wear and coatings deposited with APTES are generally hydrophilic. The coatings obtained were analyzed by Scanning Electron Microscopy (SEM), Atomic Force Microscopy (AFM), Fourier Transform Infra-Red (FTIR) spectroscopy, X-ray Photoelectron Spectroscopy (XPS), static Water Contact Angle (WCA) measurements, tribological ball-on-disc tests and contact profilometry. A relationship between the achievement of a hydrophobic character and the modifications to roughness and surface morphology and the incorporation of fluorocarbon groups in the surface chemistry was observed. Also, it was seen that the wear resistance was influenced by the SiOSi content of the coatings. In turn, the SiOSi content appears to be direct related to the percentage of APTES used in the mixture of precursors. The best conjunction of hydrophobicity and wear resistance in this work was found in the sample that was coated using a mixture of APTES and PFH in proportions of 75% and 25%, respectively. Its WCA ($100.2^{o} \pm 7.5$) was the highest of all samples that were measured and more than three times that of the uncoated glass ($31^{o} \pm 0.7$). This sample underwent a change from a hydrophilic to a hydrophobic character. It also had the lowest wear rate of the hydrophobic samples obtained in this work, with a reduction of 28.8% in the wear rate of the uncoated glass.

Keywords: Hydrophobicity, Wear resistance, Aminopropyltriethoxysilane, Perfluorohexene, Non-thermal atmospheric jet plasma, Plasma-polymerization

1. INTRODUCTION

Many recent research studies have examined the attainment and enhancement of a hydrophobic character on the surface of different materials [1-3]. Furthermore, one of the ways to develop hydrophobic surfaces that is attracting great interest from researchers is the deposition of hydrophobic coatings by atmospheric plasma [4-11]. A highly hydrophobic character is desirable for many products and industrial uses, such as self-cleaning fabrics, friction reduction in microfluidic devices, self-cleaning glass for windows, windshields and solar panels, etc. [4]. Midtdal and Jelle [12] pointed out the importance of investigating and developing superhydrophobic surfaces, with water contact angles (WCA) of more than 150º, given the excellent self-cleaning ability that these particular cases have shown. Terriza et al. [1] assessed the influence of surface chemical composition and surface roughness on wettability, using chemical vapor deposition of diamond-like carbon and fluorocarbon materials on different substrates. They found a direct correlation between roughness and water contact angles, whereas superhydrophobic behavior was found only for films having the highest fluorine content that were deposited on very rough substrates. Both chemical composition and surface roughness are critical factors in controlling the wettability of these surfaces. So, two different ways, or a combination of both, can be followed to enhance the hydrophobicity of a surface: (1) modifying the chemical composition of a rough surface with low-surface-energy materials or (2) generating a rough surface morphology on an intrinsically hydrophobic substrate [2].

Glass is a material that is used for many external applications, such as windows used in vehicles and in architecture [13], as well as in photovoltaic cells and parabolic mirrors for photothermal plants in the field of renewable energy. Solar panels have a theoretical efficiency limit of about 33.7% [12]. Therefore, it is very important to utilize the full

capability of these elements by approaching that limit as closely as possible. The main problems that the glass surfaces of solar panels encounter are deterioration caused by weather, cleaning or maintenance work, and deposition of dirt and snow. These factors cause the surface to gradually become more opaque and, as a result, to reduce the efficiency of the solar panels. Because of the foregoing, this work aims to deposit a coating that promotes a hydrophobic character and enhances the wear resistance of glass surfaces.

Wu et al. [14] prepared coatings on glass substrates and silicon wafers by microwave plasma-enhanced chemical vapor deposition (CVD) of trimethylmethoxysilane (TMMOS) with CO_2, followed by a CVD treatment using heptadecafluoro-1,1,2,2-tetrahydro-decyl-1-trimethoxysilane (FAS17) as a precursor to increase the hydrophobicity. Their optimal coating had a WCA of 150º and a wear depth that was lower than that of the glass substrate. In our work, the study of wear resistance is carried out under more severe conditions by obtaining the wear rate of our samples after conducting tribological ball-on-disc tests at a load of 1 N.

The use of two liquid precursors and mixtures of both in different proportions will be considered for the deposition of the coatings analyzed in this work. 1-perfluorohexene (PFH) is a low-surface-energy precursor with a molecule that consists of a fluorocarbon chain. It is assumed that this type of fluorocarbon material, which is rich in fluorine, tends to be hydrophobic because of the low reactivity of the C-F bonds exposed at the surface [1]. However, the low reactivity and low surface energy of these materials may be a drawback from the point of view of adhesion to the substrate [15]. Consequently, a combination of the fluorinated precursor and an additive that facilitates adhesion and governs the mechanical behavior of the coating is advisable [16]. For this purpose, aminopropyltriethoxysilane (APTES) will also be used as precursor. This aminosylane is often used in silica surface functionalization with amine groups. Aminosylanes are useful in binding proteins or other molecules to glass or silicon dioxide surfaces [17]. The deposition of coatings with

aminosylanes often results in the formation of siloxane (SiOSi). Masuko et al. [18] analyzed the tribological properties of smooth silicon substrates coated with self-assembled monolayers (SAMs) that contained different amounts of siloxane bonds. Their results revealed that the SAMs with a higher content of siloxane bonds had lower and more stable friction coefficients, and provided longer durability than coatings that contained lower amounts of siloxane bonds. Thus, we used APTES to facilitate the sticking of the hydrophobic coating and to enhance the wear resistance of the surface.

Plasma deposition permits the formation of coatings that have different functional properties by a low temperature process on a wide range of substrates. As a consequence, it has gained interest over the last 50 years. The use of non-equilibrium vacuum plasma systems during these years has led to the development recently of techniques of atmospheric plasma pressure coating. The use of plasma at atmospheric pressure enables these techniques to be low in cost, easy to operate and easy to integrate for in-line processing. Furthermore, monomers with very different chemical natures can be copolymerized using plasma [19].

There are different possibilities to deposit coatings with various functional properties by plasma-polymerization. One of them could be the deposition of alternating layers using separately one precursor or another for each layer. This possibility was discarded since it was intended that the upper layer had simultaneously both target properties (hydrophobicity and wear resistance). Another possibility is the simultaneous application of the previously mixed precursors. This method consists in the preparation of a mixture of both precursors by putting them together into the container for the precursor of the plasma system. This mixture can be carried by a flow of gas to be atomized and deposited by plasma-polymerization. Thus, changing only the content of the container and keeping unvaried the rest of the system and process, the plasma-polymerization of a single precursor or mixtures of different precursors can be carried out. This method has been tested in previous work of this research group [6,7] and it has allowed obtaining coatings that combine the features of the precursors used.

For these reasons, the use of a non-thermal atmospheric jet plasma system to deposit mixtures of two liquid precursors (APTES and PFH) is considered to be a suitable option for the present work.

Therefore, we will analyze different coatings deposited by plasma-polymerization of APTES and PFH by a non-thermal atmospheric jet plasma system on glass substrates. With the objective of finding a coating that provides the most balanced enhancement of both hydrophobicity and wear resistance, the two liquid precursors will be used individually and in mixtures of different proportions.

2. MATERIALS AND METHODS

The substrates used in this work were glass samples of 100 mm × 50 mm × 3.9 mm in dimensions. A PlasmaSpot® [20] system of non-thermal atmospheric jet plasma was used to coat the samples. It was equipped with a plasma torch system at atmospheric pressure, which includes an Al_2O_3 dielectric barrier between two cylindrical electrodes, operating in a jet. The distance between the substrate and the jet was fixed at 6 mm, and the movement of the jet over the surface of the sample was set at a constant speed of 6 m/min and 2 mm of track pitch. The process applied consisted of two phases. The first phase was a surface activation treatment in which no precursor was used and samples were subjected to one pass of plasma treatment. This activation phase was applied to all samples that were coated subsequently, as well as to one sample that was kept uncoated to remove its surface contamination and use as a reference for chemical characterization. The second phase consisted of coating the samples by plasma-polymerization in two passes. The supply gas used for the two phases was nitrogen (99.99%) at a flow rate of 80 slm. The generator's power was set at 450 W and the frequency at 68 kHz. Two liquid precursors were used to coat the samples. They were aminopropyltriethoxysilane (APTES, $H_2N(CH2)_3Si(OC_2H_5)_3$) and 1-perfluorohexene (PFH, $CF_2=CF(CF_2)_3CF_3$). Table 1 shows the proportions in which both precursors were mixed for each analyzed sample.

The precursors were placed into the same container in the proportions associated with each sample type prior to atomization. The precursors were carried by nitrogen gas at a flow rate of 1.5 slm through an atomizer (TSI model 3076) to be added perpendicularly to the afterglow through a 0.5 mm opening at the end of the central tube of the jet. The flow rate of the precursor mixture that is carried by the nitrogen was about 0.06 ml/mm.

Four sub-samples of 10 mm × 10 mm × 3.9 mm in dimensions from different locations of each type of sample of 100 mm × 50 mm × 3.9 mm in dimensions were used to obtain analytical results that would be convincing. Phase-shifting interferometry (PSI) with a WYKO NT3300 non-contact surface profiler was used to measure the thickness of the coatings. The average coating thickness of four measurements from each sample was determined. A Scanning Electron Microscope (SEM) HITACHI S-2400 at 18 kV of operating voltage was used to examine the surfaces of the coated samples and the uncoated substrate, as well as the wear tracks generated by tribological tests. In order to make possible these observations by SEM, the samples were made conductive by gold sputtering.

The surface morphology of the coatings and the uncoated glass was studied also by Atomic Force Microscopy (AFM) in tapping mode using an XE-70 (Park Systems) atomic force microscope with a silicon cantilever PPP-NCHR (Nanosensors). The root mean square (RMS) values of roughness were calculated from the images obtained in scanning a 10 μm × 10 μm area of each sample.

Fourier Transform Infra-Red (FTIR) spectroscopy and X-Ray Photoelectron Spectroscopy (XPS) analyses were carried out for chemical characterization of the coatings. Silicon wafers of 1 cm^2 area were used as substrates for the FTIR analysis. Those silicon wafers were subjected to the same process that was described for the glass samples. Also, the same proportions of precursors were used, assuming that the FTIR spectra of the coatings on both substrates are the same. FTIR spectra with a resolution of 2 cm^{-1} in the range of 400-4000 cm^{-1} were averaged over 64 scans in transmission mode of each sample by a BRUKER IFS 66

FTIR spectrometer. The peak at 611 cm^{-1} that is related to the Si-Si of the substrate [21] was used to normalize the FTIR spectra of all samples. The FTIR spectrum of the activated substrate was subtracted from the spectra of the coated samples to obtain more accurate chemical characterization of the coatings. A Physical Electronics PHI 5700 spectrometer with a multi-channel hemispherical analyzer, a MgKα (1253.6 eV) X-ray source that was powered at 300W and operated at 15 kV, a pass energy of 29.35 eV and a base pressure below 1.33×10^{-7} Pa was used for the acquisition of the X-ray photoelectron spectra. Each spectrum was obtained by analyzing four sub-samples of each sample type. Adventitious carbon at a binding energy of 285 eV in the C1s signal was used to reference the peaks of all samples. The XPS photoelectron peaks were fitted with a Shirley background subtraction. The areas under these peaks were used to calculate the atomic concentrations of C, O, Si, N and F. Deconvolutions of the FTIR spectra after subtraction and of the C1s region of the XPS spectra were carried out using the PeakFit 4.12 software (SPSS Inc.) and Gaussian-Lorentzian sum functions to fit the peaks of the deconvolutions. The shape and number of peaks were constrained, whereas variable widths were allowed.

The wettability of the analyzed samples was studied by measuring the static water contact angle (WCA) by the sessile drop method. Four sub-samples of each sample type were measured. The WCA (mean ± standard deviation) of each sample type was averaged from the results that were obtained by image analysis of four water drops (3 μL/drop) placed on each sub-sample.

The frictional behavior and wear of the samples were studied by tribological tests and profilometry measurements. The tribological tests were conducted at room temperature in unlubricated conditions by a rotational ball-on-disc tribometer (CSM Instruments). The tribometer was equipped with a spherical counterpart that was 6 mm in diameter and made of 100Cr6 steel (HRC 60-62). The parameters established for the tribological tests were the following: a normal load of 1 N, a total sliding distance of 100 m at a sliding speed of 2 cm/s

and a radius of 2.5 mm. The friction coefficient (mean ± standard deviation) of each sample type was an average of the results obtained by testing four sub-samples. Four measurements of the cross-sectional area of each wear track that was generated during the tribological tests were taken by a contact profilometer Surtronic 25 (Taylor Hobson) and the mean value of the measurements for each sample type was used to calculate its wear rate.

3. RESULTS

3.1. Coating thickness and morphology

The coating thickness and surface roughness of the samples (Table 2) were obtained by interferometry and AFM images (Fig. 1) respectively. SEM analysis (Fig. 2) was used along with the AFM to study the surface morphology of the samples.

As can be seen, only the samples in which APTES was used have a noticeable coating thickness. The surface roughness, which is one of the main factors that influence the wettability [1,2], was greatly increased by using mixtures of APTES and PFH.

Fig. 1(c-e) and Fig. 2(c-e) reveal the presence of agglomerates and smaller particles on the coatings of these three samples (AP_{25}, AP_{50}, AP_{75}). However, sample AP_{100} has a smooth and uniform coating on which only very small particles can be distinguished (Fig. 1(f) and Fig. 2(f)).

The surface of sample AP_0 is characterized by the presence of a few dispersed agglomerates that are separated by smooth areas. This, along with the extremely low coating thickness of sample AP_0, indicates that most of the surface could not be coated by using only PFH.

3.2. Fourier Transform Infra-Red spectroscopy

FTIR analysis was conducted for the chemical characterization of the coatings. The FTIR spectra of the coated samples after subtraction of the spectrum of the activated substrate are shown in Fig. 3. Various regions can be distinguished on each spectrum.

In the range of 700-990 cm^{-1} (Fig. 3, region A), the spectrum of the activated substrate has peaks that can be related to SiC [6] and SiO [22] vibrations at wavenumbers of ~738 and

~817 cm^{-1}, respectively. In addition, the spectrum has some peaks in the range of 835-990 cm^{-1} that may be due to SiOH stretching [6,23,24]. All of these peaks were present in the spectra of the coated samples before subtraction. However, only a peak at ~700 cm^{-1}, which may be related to CH_2 rocking [6,23], can be identified in the range of 700-990 cm^{-1} in the spectra of the coated samples after subtraction (Fig. 3, region A).

There is a band in the range of 1000-1260 cm^{-1} (Fig. 3, region B) in which the main differences between the spectrum of the activated substrate and those of the coated samples have been found. The spectrum of the activated substrate showed only a narrow peak due to silica at ~1105 cm^{-1} [25]. The overlapping of silica by other groups from the coatings caused this band to be broader in the spectra of the coated samples. After subtraction, these other groups could be identified on both sides of the wavenumber that is related to silica. The side that is located at lower wavenumbers may be composed of SiOSi asymmetric stretching mode (ASM) at ~1035 cm^{-1} [6,16,19,24] and SiOC ring-link structures at ~1064 cm^{-1} [6,20] and becomes more intense as the percentage of APTES used increases. The side that is located at higher wavenumbers may be composed of vibrations of the following groups: (1) SiOC open-link structures at ~1115 cm^{-1} [6,20] and SiOC cage-link structures at ~1162 cm^{-1} [6,20], (2) CF_x groups (x = 1, 2, 3) at ~1149 cm^{-1} [6,16,26,27], ~1200 cm^{-1} [6,26] and ~1236 cm^{-1} [6,28] and (3) OCH_2CH_3 at ~1200 cm^{-1} [6,20], which is probably overlapped by the CF_x groups at the same wavenumber.

The oscillations of all the spectra in the range of 1400-1800 cm^{-1} (Fig. 3, region C) are probably due to the presence of residual water vapor in the spectrometer. In the subtracted spectra of the samples that were coated using APTES (AP_{25}, AP_{50}, AP_{75} and AP_{100}), these oscillations are overlapped by two peaks, one at ~1540 cm^{-1} and one at ~1660 cm^{-1}. The peak at ~1540 cm^{-1} probably is related to the Amide II band that involves N-H bending and C-N stretching [29,30]. The peak at ~1660 cm^{-1} may be related to the Amide I band and may include NH bending, C=N stretching and C=O stretching [19,29,31]. The groups formed by

nitrogen that have been identified in these peaks were originated by the amine groups provided by APTES.

There is another band in the spectra of the coated samples in the range of 2000-2300 cm^{-1} (Fig. 3, region D) that is related to Si-H groups [16,32]. This band is generally broader and more intense when higher percentages of APTES are used. While this band covers the entire range of 2000-2300 cm^{-1}in samples AP_{50}, AP_{75} and AP_{100}, it is found mainly at the highest wavenumbers of that range in samples AP_0 and AP_{25}.

A deconvolution of the spectra of the coated samples after subtraction in the range of 1000-1260 cm^{-1} (Fig. 4) was undertaken to determine the presence of the main groups identified in this range. The peak at ~1200 cm^{-1} is caused by OCH_2CH_3 [6,20], which is provided by APTES and CF_x [6,26], which is provided by PFH. In samples AP_{25}, AP_{50} and AP_{75} both groups are overlapped at the same wavenumber and, therefore, their respective contributions to this particular peak cannot be determined precisely.

In view of the influence on tribological characteristics and wettability that is attributed to the groups of SiOSi [18] and CF_x [1,6], the presence of these groups in the coatings obtained has been studied more thoroughly. Fig. 5 shows the area under the peak that is related to SiOSi (ASM) in the deconvolution (peak 1 from Fig.4) and the sum of the areas under the peaks that are related to CF_x (peaks 4+6+7 from Fig. 4). The presence of SiOSi is related to the proportion of APTES that is used. This group has not been found in sample AP_0 and the area under the corresponding peak increases in the remaining samples as the percentage of APTES that is used increases. One could expect that, by decreasing the percentage of PFH used, and thus increasing the percentage of APTES in the mixtures of precursors, there would be a lower presence of CF_x groups in the coatings. However, these variations in the percentages of the precursors have resulted in a slightly higher presence of CF_x groups in the coatings that were obtained by using lower percentages of PFH (samples AP_{50} and AP_{75}) than used in the other fluorinated coatings (samples AP_0 and AP_{25}).

3.3. X-ray Photoelectron Spectroscopy

XPS analysis was performed to determine whether there is any relationship between the proportions of the precursors used and the surface chemistry of the coatings that were obtained by plasma-polymerization. Fig. 6 shows the atomic percentages of carbon (C1s), oxygen (O1s), silicon (Si2p), nitrogen (N1s) and fluorine (F1s) on the surface of the samples analyzed.

All samples contain a noticeable percentage of carbon. This is probably caused by adventitious carbon in the case of the activated glass, and a combination of adventitious carbon with carbon that is provided by the precursors during the plasma-polymerization process that is applied to the remaining samples. The percentages of nitrogen on the samples in which APTES was not used (activated substrate and sample AP_0) is negligible, whereas the samples in which APTES was used show significant percentages of nitrogen. The percentage of fluorine is significant only on the samples that were coated using PFH (AP_0, AP_{25}, AP_{50} and AP_{75}). Furthermore, the percentages of fluorine are similar among these samples; although they decrease slightly as the percentage of PFH used increases.

Deconvolution of the C1s signal of the coated samples was carried out (Fig. 7) to develop a better quantification of the relative percentages of the fluorocarbon groups on the surfaces of these samples (Fig. 8). The functional groups and binding energies associated with all of the peaks considered in the deconvolution are shown in Table 3. The following fluorocarbon groups were found: C-CF at ~286 eV, CF at ~288 eV, CF_2 at ~291.4 eV. In the samples that were coated with mixtures of APTES and PFH, overlapping of C-N with C-CF was identified at a binding energy of ~286 eV. There is also C=O overlapped by the CF at a binding energy of ~288 eV. The most noticeable relative percentages of the three peaks that are related to fluorocarbon groups were those corresponding to the peak at ~286 eV (peak 3) in the samples that were coated by mixtures of APTES and PFH (AP_{25}, AP_{50} and AP_{75}). Although these percentages are due partially to the contribution of C-N groups that probably were formed by

nitrogen from the amine groups of APTES, one can see that peak 3 (Fig. 7(b-e)) and its relative percentage (Fig. 8) are lower in sample AP_{100} than in the samples that were coated with mixtures of APTES and PFH. From this, it follows that there is an important contribution of C-CF to this peak when mixtures of both precursors are used. The relative percentages corresponding to the other two peaks that are related to fluorocarbon groups were lower, or even zero. Therefore, it is believed that fluorocarbon groups provided by PFH could be deposited, leading to the formation of mainly C-CF.

3.4. Water Contact Angle measurements

Static water contact angle (WCA) measurements were taken to determine the wettability of the analyzed samples. The results in Fig. 9 reveal that the uncoated glass had the lowest WCA ($31^o \pm 0.7$) and had the strongest hydrophilic character (WCA < 90^o) among these samples. The samples that were prepared exclusively with one of the two precursors used in this work (samples AP_0 and AP_{100}) also exhibited a hydrophilic character. Compared to the uncoated glass, sample AP_0 had a slightly higher WCA ($40.6^o \pm 1$). The WCA of sample AP_{100} was noticeably higher ($70^o \pm 6.6$).

A hydrophobic character (WCA > 90^o) was achieved only in the samples that were prepared with mixtures of APTES and PFH (samples AP_{25}, AP_{50} and AP_{75}). Those three samples had similar WCAs, ranging from $92.5^o \pm 2.2$ for sample AP_{50} to $100.2^o \pm 7.5$ for sample AP_{75}.

3.5. Tribological characteristics

Fig. 10 shows the friction coefficient of each sample as obtained by tribological tests and the wear rates that were calculated from profilometry measurements, expressed as the mean value of the results obtained and their standard deviation.

The uncoated glass and sample AP_0 had the highest friction coefficients measured and were almost the same. When APTES is used as precursor, a reduction of the friction coefficient of the uncoated glass is obtained. Furthermore, the general trend of these results shows that the higher the percentage of APTES is, the lower the friction coefficient is. A reduction of 11.2%

in the friction coefficient of the uncoated glass was obtained by using APTES at 50% of the mixture of precursors (sample AP_{50}). This reduction reaches 16.9% when only APTES was used (sample AP_{100}).

There is a similar result with the wear rate. The uncoated glass and sample AP_0 had very similar wear rates after the tribological tests, and the highest of all wear rates obtained for the analyzed samples. When APTES was used, the wear rate was reduced. It decreases further when APTES was used in higher percentages. This is most evident in samples prepared with percentages of APTES of 50% or higher (samples AP_{50}, AP_{75} and AP_{100}), whereas the wear rate of sample AP_{25} is slightly higher, but similar to that of sample AP_{50}.

3.6. Wear processes

The wear tracks generated by the tribological tests on the surfaces of the analyzed samples were observed by SEM. Several images were examined to determine the wear processes that had taken place.

As can be seen in Fig. 11, the uncoated glass, sample AP_0 and sample AP_{25} experienced severe wear, mainly by an abrasive process. This wear process can be identified by the presence of deep grooves that are parallel to the sliding direction in the wear tracks of these samples (white arrows in Fig. 11(a-c)). In the cases of uncoated glass and sample AP_0, abrasive wear was combined with fragmentation and surface cracking (yellow arrows in Fig. 11(a, b)), which led also to material detachment by delamination. All of these processes were observed previously by other authors [36].

The wear tracks of samples AP_{50}, AP_{75} and AP_{100} have been occupied by a tribofilm (Fig. 12). The tribofilm on sample AP_{50} shows many cracks that are related to the processes of wear by delamination and fatigue (Fig. 12(a)), as other authors have observed [36]. These wear processes have resulted in material detachment from the borders of the wear track and from some locations of the central zone of the track (yellow arrows in Fig. 12(a)). Similar processes, although causing less severe wear, have occurred with sample AP_{75} (Fig. 12(b)).

Material detachment has occurred on sample AP_{75} mainly at the borders of the wear track (yellow arrows in Fig. 12(b)), whereas there is less cracked tribofilm in the central zone of the track than in sample AP_{25}. The wear track of sample AP_{100} exhibited the most continuous of all tribofilms that were observed in this work (Fig. 12(c)). No sign of cracking could be identified in this tribofilm. Incipient detachment of the tribofilm was noticed at some locations on the border of the wear track (yellow arrow in Fig. 12(c)), as well as some particles of wear debris (white arrows in Fig. 12(c)).

4. DISCUSSION

The coating thickness is noticeable only on those samples that were coated using APTES (samples AP_{25}, AP_{50}, AP_{75} and AP_{100}). A similar situation for the nitrogen percentages is observed in the XPS analysis results (Fig. 6), which are noticeable only when APTES has been used. These results are also in agreement with the groups that are formed by nitrogen in the FTIR spectra (Fig. 3). It follows that nitrogen comes mainly from the amine group that is contained in the APTES molecule. Although no strict relationship between the coating thickness and the results of chemical characterization regarding nitrogen can be seen, the growth of the coating may be favored by the presence of amine groups acting as a binder [37]; as it is suggested by the results of our previous work [6,7].

When coatings that have a noticeable thickness are obtained, their roughness and surface morphology appear to be affected by the presence of PFH in the mixtures of precursors. A smooth, uniform coating with a few small particles was obtained when only APTES was used (sample AP_{100}). In contrast, the use of mixtures of APTES and PFH led to the formation of rougher coatings with agglomerates and small particles (Fig. 1 and Fig. 2). The differences in morphology of the samples coated with mixtures of APTES and PFH may be determined by the flash point of the mixture of precursors used for each case. The flash point of a chemical is the lowest temperature at which enough fluid can evaporate to ignite in air. The different flash points of APTES (96 ºC) and PFH (-17 ºC) can influence the flash point of each mixture. So,

the higher the proportion of PFH is, the lower the flash point of the mixture is. As other authors have observed [38], there is a higher degree of plasma-polymerization in the gas phase as the flash point of the mixture of precursors decreases. Thus, the surface of sample AP_{75} (Fig. 1(e)) is composed mainly of agglomerates and some spherical particles that were formed by polymerization in the gas phase [39,40]. The higher the percentage of PFH used in the mixtures is (samples AP_{50} and AP_{25}), the higher the degree of plasma-polymerization in the gas phase is. This leads to an increase in the amount of particles formed and a decrease in the size of the agglomerates as the percentage of PFH used in the mixture of precursors increases (Fig.1 (c-e)). Furthermore, the surface of sample AP_{25} (Fig. 1(c)) has plenty of dusty-like particles of fluorocarbon [41,42] provided by PFH. Such particles were formed by polymerization in the gas phase [40].

The use of higher percentages of PFH provides more fluorine for the plasma-polymerization process. However, the lower flash point of PFH makes the material more volatile and more likely to be evacuated by the exhaust whereas the presence of lower amounts of amines may hinder its capability of adhering to the substrate. Therefore, the decrease in the flash-point of the mixture and in the amount of amines provided by APTES could be why the percentages of fluorine in the fluorinated samples were lower as the percentage of PFH used increased.

The extremely low coating thickness of sample AP_0 and the results obtained for sample AP_0 in many of the analyses that were similar to the results obtained for the uncoated substrate, reveal that most of sample AP_0 remained uncoated. This is probably because the absence of amines in this case prevented most of the material from adhering to the substrate. It thus was evacuated by the exhaust. This assumption is supported by the results of FTIR analysis in which a noticeable presence of fluorocarbon groups was observed only if PFH had been mixed with APTES.

As mentioned above, wettability is influenced by two main factors, namely surface morphology and surface chemistry [1,2]. Only the samples that were coated by using mixtures

of APTES and PFH (AP_{25}, AP_{50}, AP_{75}) showed a hydrophobic character (WCA > 90º). These three samples were the roughest ones (Table 2) and had similar surface morphologies (Fig. 1(c-e)). These samples also had the highest content of fluorocarbon groups, although this content seemed to increase slightly as the percentage of PFH used in the mixture decreased, as shown by the results of FTIR (Fig. 5) and XPS (Fig. 8) analyses. So, although the roughness of sample AP_{75} was not the highest that was measured on these samples, the incorporation of CF_x groups that were observed in sample AP_{75} may have caused its WCA to be the highest of those measured in this work, although only slightly higher than the WCA of the other hydrophobic samples (Fig. 9).

All of the hydrophilic samples (uncoated glass, AP_0 and AP_{100}) were smooth (Table 2 and Fig. 1(a,b,f)) and their chemistry varied (Fig. 6) depending on whether a precursor was used and its type (PFH or APTES). The WCA measured on sample AP_0 was slightly higher than that of the uncoated glass. This could be due to the incorporation of a small amount of fluorocarbon groups in sample AP_0 (Fig. 5 and Fig. 8), although most of this sample remained uncoated. The WCA measured on sample AP_{100} was considerably higher than those on the uncoated glass and sample AP_0. This may be due to the chemistry of the coating of sample AP_{100}, which contains non-polar CH_3 groups from APTES [3].

Considering the differences between the triplet of hydrophilic samples (uncoated glass, AP_0 and AP_{100}) and the triplet of hydrophobic samples (AP_{25}, AP_{50}, AP_{75}), we conclude that a hydrophobic character was achieved by changes in both factors - generating rough surface morphologies and incorporating fluorocarbon groups in the surface chemistry. Furthermore, the differences in the WCA among the samples belonging to the same triplet can be explained by the differences in their surface chemistry.

The friction coefficient and the wear rate of the analyzed samples show similar trends (Fig. 10). The highest values obtained were those for the uncoated glass and sample AP_0. They decreased for the remaining samples as the percentage of APTES that was used increased.

Both can be related to the presence of SiOSi groups that were identified by FTIR analysis (Fig. 5), which increases as the percentage of APTES that is used increases. This is consistent with the findings of other authors [18], who have observed that the presence of SiOSi groups can be related to the tribological characteristics of the coatings obtained, such as lower friction coefficients and higher wears resistance.

The wear process of the surface was changed from primarily abrasive wear to a less severe wear that was governed by the formation of a tribofilm on the samples that were coated using percentages of APTES of 50% or higher. The typical stages of tribofilm formation [43,44] can be described as follows: The surface undergoes severe wear in the beginning, which generates grains and particles of wear debris. Part of this debris can be ejected from the contact zone, but the debris that remains in this zone is subjected to grinding, agglomeration and smashing during successive cycles by the counterpart. This process results in the formation of a film on the worn surface that is known as tribofilm. This tribofilm protects the surface and reduces the severe wear that took place in the beginning, thereby achieving a decrease in the wear rate and the friction coefficient [43,45].

The tribofilm of sample AP_{50} (Fig. 12(a)) was cracked and detached from several locations in the inner zone of the wear track at the end of the tribological tests. This caused the wear rate of this sample to be similar to that of sample AP_{25} (Fig. 11(c)). However, the tribofilm of sample AP_{50} produced the most noticeable decrease in the friction coefficient between two consecutive samples observed in this work. The tribofilms of samples AP_{75} and AP_{100} (Fig. 12(b, c)) were more continuous and remained less cracked until the end of the tribological tests. This could explain why the lowest values of friction coefficient and wear rate (Fig. 10) corresponded to these samples [46].

5. CONCLUSIONS

In this work, two liquid precursors (APTES and PFH) were used individually and mixed in different proportions in a non-thermal atmospheric jet plasma-polymerization system to obtain a coating that promotes wear resistance and bestows a hydrophobic character to glass. The modification of surface morphology and roughness, combined with the incorporation of fluorocarbon groups in the surface chemistry, provided a hydrophobic character (WCA > 90º) on the samples that were coated using mixtures of both precursors (samples AP_{25}, AP_{50} and AP_{75}). These three samples showed agglomerates on their surfaces and the highest values of roughness, as well as the highest contents of fluorocarbon groups that were observed in this work.

Amines from APTES favored the growth of the coatings, allowing the formation of coatings with noticeable thicknesses only when this precursor was used. The wear resistance and friction coefficient of the coatings are related to their SiOSi content. In turn, the SiOSi content of the coating is directly related to the percentage of APTES used. Therefore, as the percentage of APTES used increases, the wear resistance increases and the friction coefficient decreases. However, using only this precursor results in a hydrophilic coating due to the smooth surface obtained and the chemical nature of APTES. The wear process was changed from primarily an abrasive process to a process that is governed by the formation of a tribofilm on the samples that were coated using APTES at a proportion of a 50% or more. This tribofilm is formed by wear debris, and protects the surface against further wear. The effectiveness of the tribofilms that were observed in this work is aided by their continuity. In turn, that is related to the percentage of APTES used.

Sample AP_{75} shows the highest value of WCA of all samples measured and the lowest wear rate of the hydrophobic samples obtained. Consequently, we conclude that sample AP_{75} was the sample that showed the best conjunction of target properties of any sample that was studied in this work. In comparison, the WCA of sample AP_{75} ($100.2^{o} \pm 7.5$) was more than

three times that of the uncoated glass (WCA of 31º ± 0.7) and the wear rate of sample AP_{75} was 28.8% less than the wear rate of the uncoated glass.

Future research will focus on improving the present results of hydrophobicity and wear resistance by testing the use of different precursors and mixtures of precursors. Furthermore, the goal of that research will be to find a coating that has a more effective conjunction of surface chemistry and morphology, in order to achieve superhydrophobicity (WCA > 150º).

Acknowledgements

This work was funded by the Regional Research Plan of the Autonomous Community of La Rioja (Spain) through project ADER 2014-I-IDD-00089. The author E. Sainz-García thanks the program of pre-doctoral contracts for the training of research staff funded by the University of La Rioja.

REFERENCES

[1] A. Terriza, R. Álvarez, A. Borrás, J. Cotrino, F. Yubero, A.R. González-Elipe, Roughness assessment and wetting behavior of fluorocarbon surfaces, J. Colloid Interface Sci. 376 (2012) 274-282.

[2] H. Ji, G. Chen, J. Yang, J. Hu, H. Song, Y. Zhao, A simple approach to fabricate stable superhydrophobic glass surfaces, Appl. Surf. Sci. 266 (2013) 105-109.

[3] M.S. Kavale, D.B. Mahadik, V.G. Parale, P.B. Wagh, S.C. Gupta, A.V. Rao, H.C. Barshilia, Optically transparent, superhydrophobic methyltrimethoxysilane based silica coatings without silylating reagent, Appl. Surf. Sci. 258 (2011) 158-162.

[4] D.J. Marchand, Z.R. Dilworth, R.J. Stauffer, E. Hsiao, J.-H. Kim, J.-G. Kang, S.H. Kim, Atmospheric rf plasma deposition of superhydrophobic coatings using tetramethylsilane precursor, Surf. Coat. Technol. 234 (2013) 14-20.

[5] J.H. Yim, V. Rodríguez-Santiago, A.A. Williams, T. Gougousi, D.D. Pappas, J.K. Hirvonen, Atmospheric pressure plasma enhanced chemical vapor deposition of hydrophobic coatings using fluorine-based liquid precursors, Surf. Coat. Technol. 234 (2013) 21-32.

[6] R. Múgica-Vidal, F. Alba-Elías, E. Sainz-García, J. Ordieres-Meré, Atmospheric plasma-polymerization of hydrophobic and wear-resistant coatings on glass substrates, Surf. Coat. Technol. 259 (2014) 374-385.

[7] E. Sainz-García, F. Alba-Elías, R. Múgica-Vidal, A. González-Marcos, Enhanced surface friction coefficient and hydrophobicity of TPE substrates using an APPJ system, Appl. Surf. Sci. 328 (2015) 554-567.

[8] F. Fanelli, A.M. Mastrangelo, F. Fracassi, Aerosol-assisted atmospheric cold plasma deposition and characterization of superhydrophobic organic-inorganic nanocomposite thin films, Langmuir 30 (2014) 857-865.

[9] S.-H. Yang, C.-H. Liu, C.-H. Su, H. Chen, Atmospheric-pressure plasma deposition of SiO_x films for super-hydrophobic application, Thin Solid Films 517 (2009) 5284-5287.

[10] Y.-Y. Ji, S.-S. Kim, O.-P. Kwon, S.-H. Lee, Easy fabrication of large-size superhydrophobic surfaces by atmospheric pressure plasma polymerization with non-polar aromatic hydrocarbon in an in-line process, Appl. Surf. Sci. 255 (2009) 4575-4578.

[11] Y.-Y. Ji, Y.-C. Hong, S.-H. Lee, S.-D. Kim, S.-S. Kim, Formation of super-hydrophobic and water-repellency surface with hexamethyldisiloxane (HMDSO) coating on polyethyleneteraphtalate fiber by atmosperic pressure plasma polymerization, Surf. Coat. Technol. 202 (2008) 5663-5667.

[12] K. Midtdal, B.P. Jelle, Self-cleaning glazing products: A state-of-the-art review and future research pathways, Sol. Energy Mater. Sol. Cells 109 (2013) 126-141.

[13] J. Abenojar, M.A. Martínez, N. Encinas, F. Velasco, Modification of glass surfaces adhesion properties by atmospheric pressure plasma torch, Int. J. Adhes. Adhes. 44 (2013) 1-8.

[14] Y. Wu, M. Bekke, Y. Inoue, H. Sugimura, H. Kitaguchi, C. Liu, O. Takai, Mechanical durability of ultra-water-repellent thin film by microwave plasma-enhanced CVD, Thin Solid Films 457 (2004) 122-127.

[15] S.H. Yang, C.-H. Liu, W.-T. Hsu, H. Chen, Preparation of super-hydrophobic films using pulsed hexafluorobenzene plasma, Surf. Coat. Technol. 203 (2009) 1379-1383.

[16] J. Carpentier, G. Grundmeier, Chemical structure and morphology of thin bilayer and composite organosilicon and fluorocarbon microwave plasma polymer films, Surf. Coat. Technol. 192 (2005) 189-198.

[17] A.R. Yadav, R. Sriram, J.A. Carter, B.L. Miller, Comparative study of solution-phase and vapor-phase deposition of aminosilanes on silicon dioxide surfaces, Mater. Sci. Eng. C 35 (2014) 283-290.

[18] M. Masuko, H. Miyamoto, A. Suzuki, Tribological characteristics of self-assembled monolayer with siloxane bonding to Si surface, Tribol. Int. 40 (2007) 1587-1596.

[19] M. Bashir, J.M. Rees, S. Bashir, W.B. Zimmerman, Microplasma copolymerization of amine and Si containing precursors, Thin Solid Films 564 (2014) 186-194.

[20] F. Alba-Elías, E. Sainz-García, A. González-Marcos, J. Ordieres-Meré, Tribological behaviour of plasma-polymerized aminopropyltriethoxysilane films deposited on thermoplastic elastomers substrates, Thin Solid Films 540 (2013) 125-134.

[21] Y. Matsui, S. Adachi, Optical properties of porous silicon layers formed by electroless photovoltaic etching, ECS J. Solid State Sci. Technol. 1 (2012) R80-R85.

[22] V.M. Gun'ko, O. Seledets, J. Skubiszewska-Zięba, V.I. Zarko, R. Leboda, W. Janusz, S. Chibowski, Phosphorus-containing carbon deposits on silica gel Si-100, Microporous and Mesoporous Mater. 87 (2005) 133-145.

[23] F. Alba-Elías, J. Ordieres-Meré, A. González-Marcos, Deposition of thin-films on EPDM substrate with a plasma-polymerized coating, Surf. Coat. Technol. 206 (2011) 234-242.

[24] J. Schäfer, R. Foest, A. Quade, A. Ohl, J. Meichsner, K.D. Weltmann, Carbon-free SiO_x films deposited from octamethylcyclotetrasiloxane (OMCTS) by an atmospheric pressure plasma jet (APPJ), Eur. Phys. J. D 54 (2009) 211-217.

[25] G. Osei-Prempeh, H.-J. Lehmler, A.-F. Miller, B.L. Knutson, S.E. Rankin, Fluorocarbon and hydrocarbon functional group incorporation into nanoporous silica employing fluorinated and hydrocarbon surfactants as templates, Microporous and Mesoporous Mater. 129 (2010) 189-199.

[26] C.-L. Li, C.-Y. Tu, J.-S. Huang, Y.-L. Liu, K.-R. Lee, J.-Y. Lai, Surface modification and adhesion improvement of expanded poly(tetrafluoroethylene) films by plasma graft polymerization, Surf. Coat. Technol. 201 (2006) 63-72.

[27] M. Okubo, M. Tahara, N. Saeki, T. Yamamoto, Surface modification of fluorocarbon polymer films for improved adhesion using atmospheric-pressure nonthermal plasma graft-polymerization, Thin Solid Films 516 (2008) 6592-6597.

[28] Y. Guo, J. Zhang, J. Xu, J. Yu, Variable morphology of PTFE-like polymer nanocrystals fabricated by oriented plasma polymerization at atmospheric pressure, Appl. Surf. Sci. 254 (2008) 3408-3411.

[29] D.K. Chattopadhyay, D.C.Webster, Hybrid coatings from novel silane-modified glycidyl carbamate resins and amine crosslinkers, Prog. Org. Coat. 66 (2009) 73-85.

[30] M.R. Chashmejahanbin, H. Daemi, M. Barikani, A. Salimi, Noteworthy impacts of polyurethane-urea ionomers as the efficient polar coatings on adhesion strength of plasma treated polypropylene, Appl. Surf. Sci. 317 (2014) 688-695.

[31] D. Mangindaan, W.-H. Kuo, C.-C. Chang, S.-L. Wang, H.-C. Liu, M.-J. Wang, Plasma polymerization of amine-containing thin films and the studies on the deposition kinetics, Surf. Coat. Technol. 206 (2011) 1299-1306.

[32] D. Rouchon, N. Rochat, F. Gustavo, A. Chabli, O. Renault, P. Besson, Study of ultrathin silicon oxide films by FTIR-ATR and ARXPS after wet chemical cleaning processes, Surf. Interface Anal. 34 (2002) 445-450.

[33] Y. Pihosh, H. Biederman, D. Slavinska, J. Kousal, A. Choukourov, M. Trchova, A. Mackova, A. Boldyryeva, Composite SiO_x/fluorocarbon plasma polymer films prepared by r.f. magnetron sputtering of SiO_2 and PTFE, Vacuum 81 (2006) 38-44.

[34] S. Schmidt, C. Goyenola, G.K. Gueorguiev, J. Jensen, G. Greczynski, I.G. Ivanov, Z. Czigány, L. Hultman, Reactive high power impulse magnetron sputtering of CF_x thin films in mixed Ar/CF_4 and Ar/C_4F_8 discharges, Thin Solid Films 542 (2013) 21-30.

[35] M. Pantoja, N. Encinas, J. Abenojar, M.A. Martínez, Effect of tetraethoxysilane coating on the improvement of plasma treated polypropylene adhesion, Appl. Surf. Sci. 280 (2013) 850-857.

[36] A. Dasari, Z.-Z. Yu, Y.-W. Mai, Fundamental aspects and recent progress on wear/scratch damage in polymer nanocomposites, Mater. Sci. Eng. R 63 (2009) 31-80.

[37] C. Volcke, R.P. Gandhiraman, V. Gubala, J. Raj, Th. Cummins, G. Fonder, R.I. Nooney, Z. Mekhalif, G. Herzog, S. Daniels, D.W.M. Arrigan, A.A. Cafolla, D.E. Williams, Reactive amine surfaces for biosensor applications, prepared by plasma-enhanced chemical vapour modification of polyolefin materials, Biosens. Bioelectron. 25 (2010) 1875-1880.

[38] C.E. Nwankire, G. Favaro, Q.-H. Duong, D.P. Dowling, Enhancing the mechanical properties of superhydrophobic atmospheric pressure plasma deposited siloxane coatings, Plasma Process. Polym. 8 (2011) 305-315.

[39] A. Michelmore, P. Martinek, V. Sah, R.D. Short, K. Vasilev, Surface morphology in the early stages of plasma polymer film growth from amine-containing monomers, Plasma Process. Polym. 8 (2011) 367-372.

[40] K. Takahashi, K. Tachibana, Solid particle production in fluorocarbon plasmas. I. Correlation with polymer film deposition, J. Vac. Sci. Technol. A 19 (2001) 2055-2060.

[41] D. Liu, W. Li, Z. Feng, X. Tan, B. Chen, J. Niu, Y. Liu, Plasma enhanced CVD of fluorocarbon films by low-pressure dielectric barrier discharge, Surf. Coat. Technol. 203 (2009) 1231-1236.

[42] I.P. Vinogradov, A. Dinkelmann, A. Lunk, Deposition of fluorocarbon polymer films in a dielectric barrier discharge (DBD), Surf. Coat. Technol. 174-175 (2003) 509-514.

[43] H. Kato, K. Komai, Tribofilm formation and mild wear by tribo-sintering of nanometer-sized oxide particles on rubbing steel surfaces, Wear 262 (2007) 36-41.

[44] J. Olofsson, S. Jacobson, The influence of grain size and surface treatment on the tribofilm formation on alumina components, Wear 292-293 (2012) 17-24.

[45] M.-S. Suh, Y.-H. Chae, S.-S. Kim, Friction and wear behavior of structural ceramics sliding against zirconia, Wear 264 (2008) 800-806.

[46] P.S. Tantri, E.M. Jayasingh, S.K. Biswas, S.K. Ramasesha, Role of in situ generated tribofilm on the tribological characteristics of monolith and TiB_2 reinforced $MoSi_2$ intermetallic, Mater. Sci. Eng. A 336 (2002) 64-71.

LIST OF FIGURE CAPTIONS

Fig. 1. AFM images of the studied samples.

Fig. 2. SEM images of the studied samples at a magnification of x5000.

Fig. 3. FTIR spectra of the activated substrate and the coated samples in the range of 500-2500 cm^{-1}.

Fig. 4. Deconvolution of the FTIR spectra of the coated samples after subtraction in the range of 1000-1260 cm^{-1}.

Fig. 5. The area under the peak related to SiOSi and the total area related to CF_x in the deconvolution of the FTIR spectra of the coated samples in the range of 1000-1260 cm^{-1} after subtraction.

Fig. 6. Atomic percentages of the main elements found on the surface of the samples by XPS.

Fig. 7. Deconvolution of the XPS spectra (C1s) of the coated samples.

Fig. 8. Relative percentages of the fluorocarbon groups identified in the C1s signal of the coated samples.

Fig. 9. Static water contact angle on the surfaces of the uncoated glass and the coated samples.

Fig. 10. Friction coefficient and wear rate of the analyzed samples.

Fig. 11. SEM images of the wear tracks of (a) the uncoated glass and samples (b) AP_0 and (c) AP_{25} at a magnification of x600. The sliding direction of the counterpart over the samples is indicated by dashed arrows.

Fig. 12. SEM images of the wear tracks of samples (a) AP_{50}, (b) AP_{75} and (c) AP_{100} at a magnification of x600. The sliding direction of the counterpart over the samples is indicated by dashed arrows.

LIST OF TABLE CAPTIONS

Table 1. Designation of the samples and their associated proportions of APTES and PFH.

Table 2. Coating thickness and RMS roughness of the studied samples.

Table 3. Functional groups and binding energies associated with the peaks considered in the deconvolution of the XPS spectra (C1s).

FIGURES AND TABLES

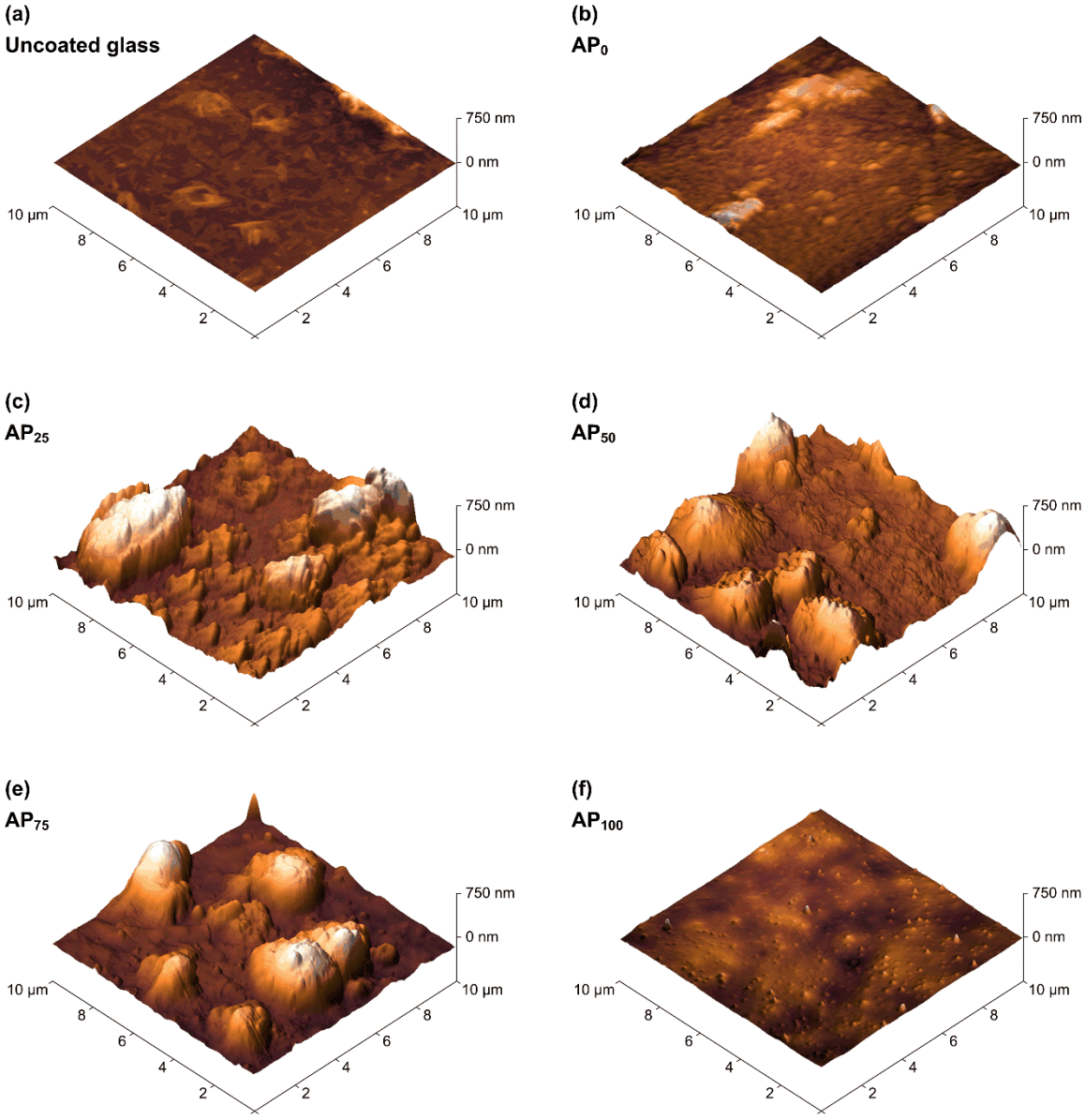

Fig. 1

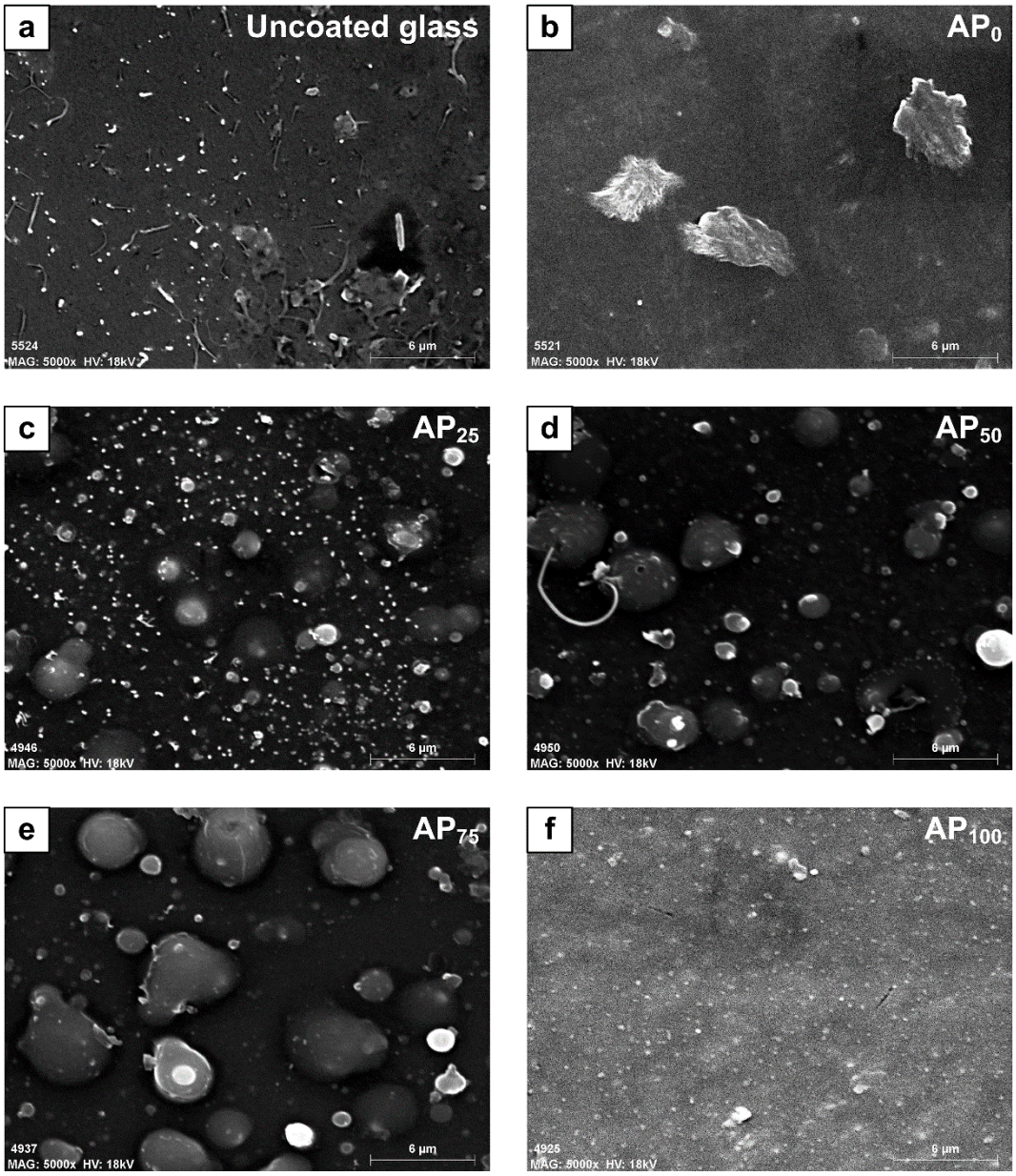
a
Uncoated glass
5524
MAG: 5000x HV: 18kV
6 µm
b
AP0
5521
MAG: 5000x HV: 18kV
6 µm
c
AP25
4946
MAG: 5000x HV: 18kV
6 µm
d
AP50
4950
MAG: 5000x HV: 18kV
6 µm
e
AP75
4937
MAG: 5000x HV: 18kV
6 µm
f
AP100
4925
MAG: 5000x HV: 18kV
6 µm

Fig. 2

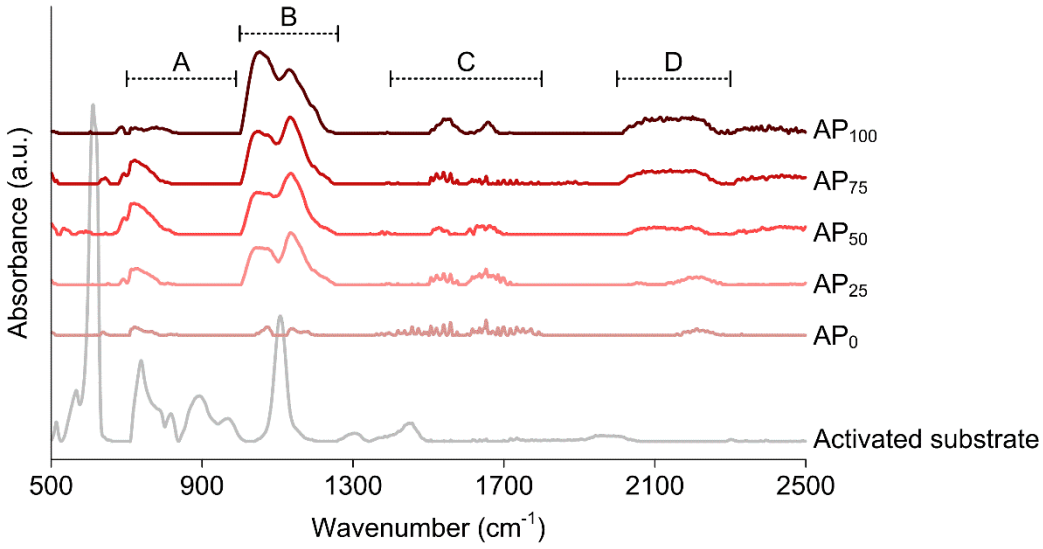
A
B
C
D
AP100
AP75
AP50
AP25
AP0
Activated substrate
Absorbance (a.u.)
500
900
1300
1700
2100
2500
Wavenumber (cm-1)

Fig. 3

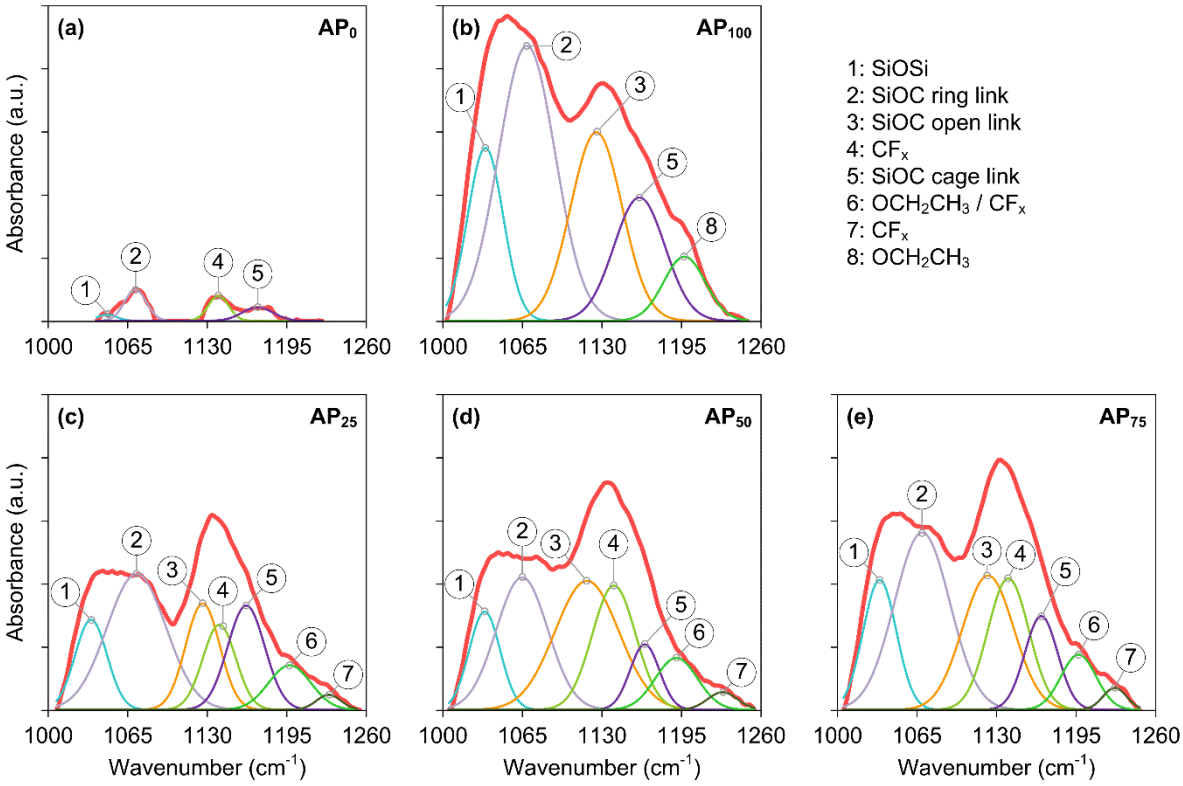
(a) AP0
(b) AP100
(c) AP25
(d) AP50
(e) AP75
Absorbance (a.u.)
1000
1065
1130
1195
1260
Wavenumber (cm-1)
1: SiOSi
2: SiOC ring link
3: SiOC open link
4: CFx
5: SiOC cage link
6: OCH2CH3 / CFx
7: CFx
8: OCH2CH3

Fig. 4

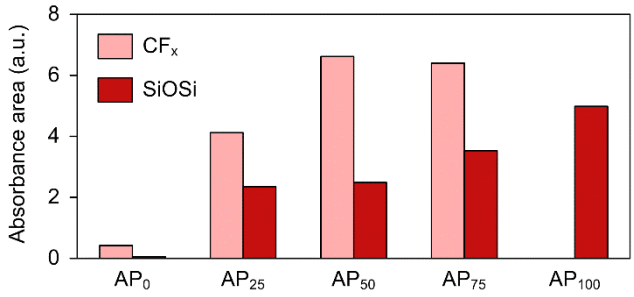
Absorbance area (a.u.)
8
6
4
2
0
CFx
SiOSi
AP0
AP25
AP50
AP75
AP100

Fig. 5

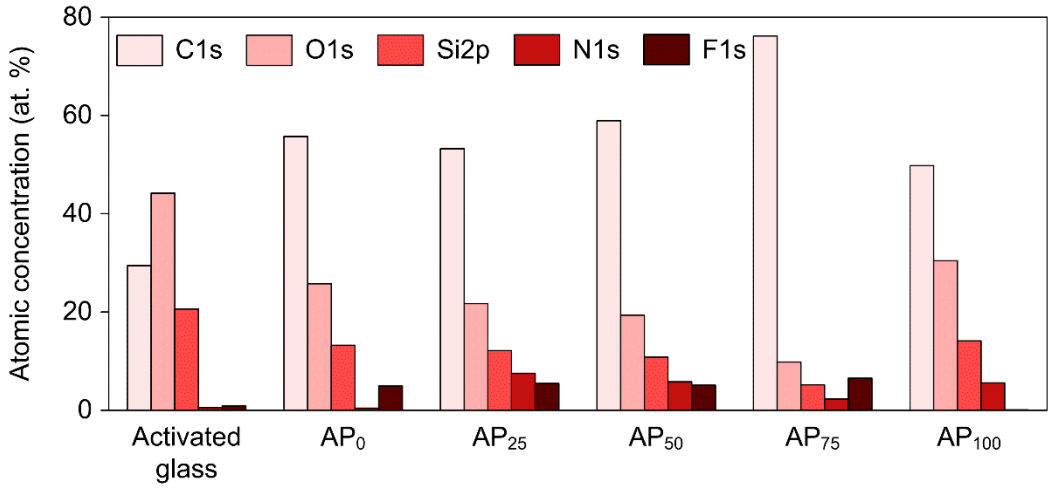
Atomic concentration (at. %)
80
60
40
20
0
C1s
O1s
Si2p
N1s
F1s
Activated glass
AP0
AP25
AP50
AP75
AP100

Fig. 6

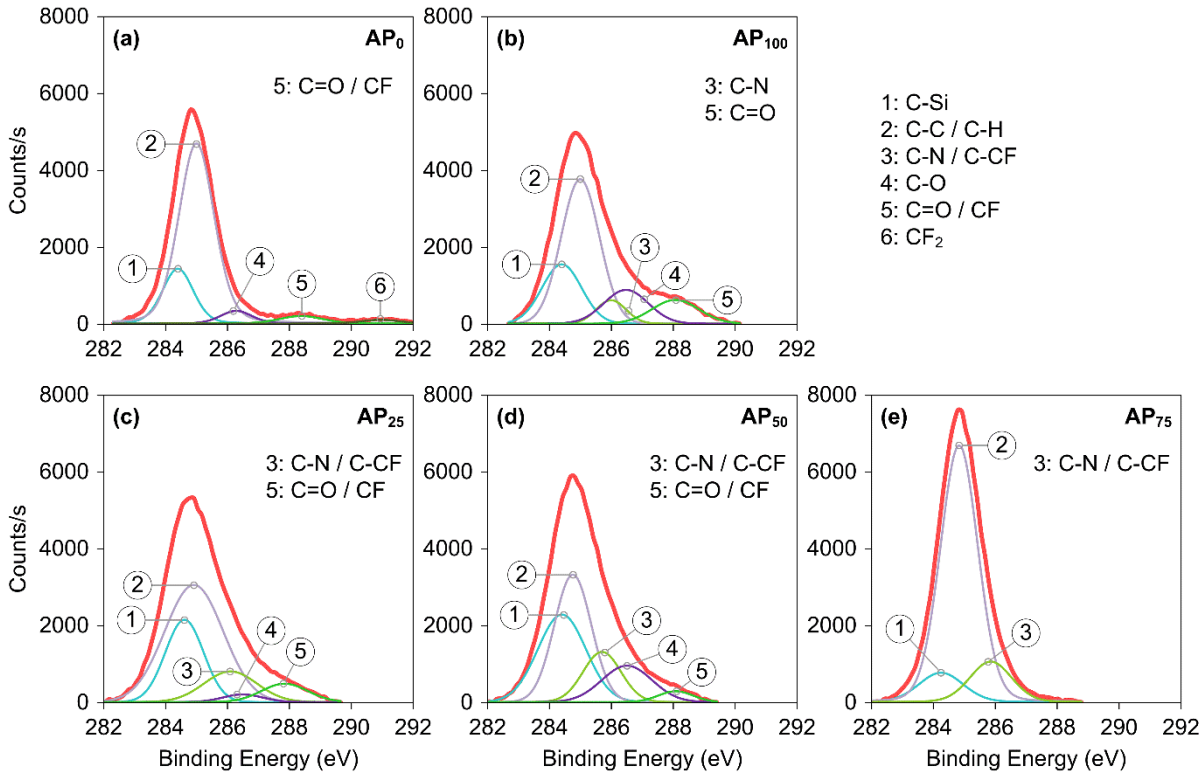
(a) AP0
5: C=O / CF
(b) AP100
3: C-N
5: C=O
(c) AP25
3: C-N / C-CF
5: C=O / CF
(d) AP50
3: C-N / C-CF
5: C=O / CF
(e) AP75
3: C-N / C-CF
1: C-Si
2: C-C / C-H
3: C-N / C-CF
4: C-O
5: C=O / CF
6: CF2
Counts/s
Binding Energy (eV)

Fig. 7

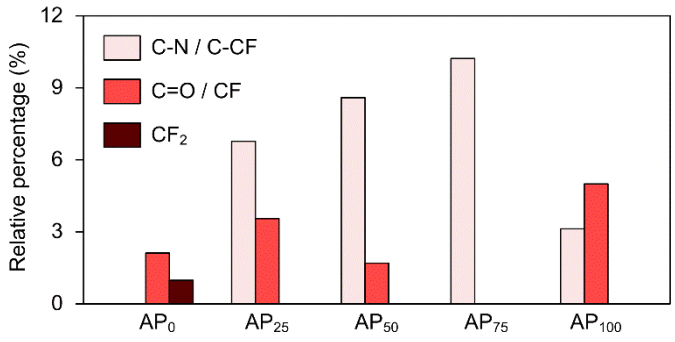
C-N / C-CF
C=O / CF
CF2
Relative percentage (%)
AP0
AP25
AP50
AP75
AP100

Fig. 8

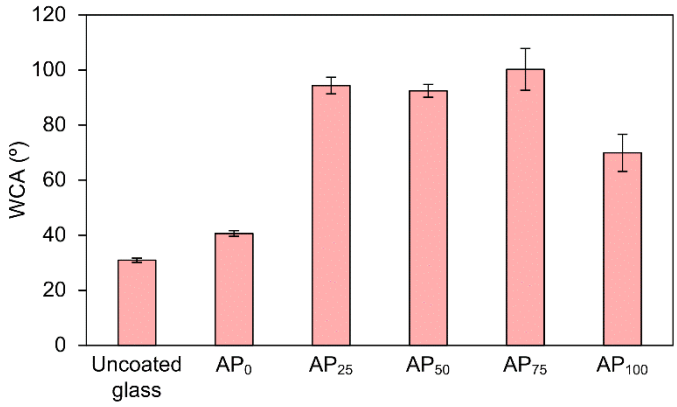
120
100
80
60
40
20
0
WCA (°)
Uncoated glass
AP0
AP25
AP50
AP75
AP100

Fig. 9

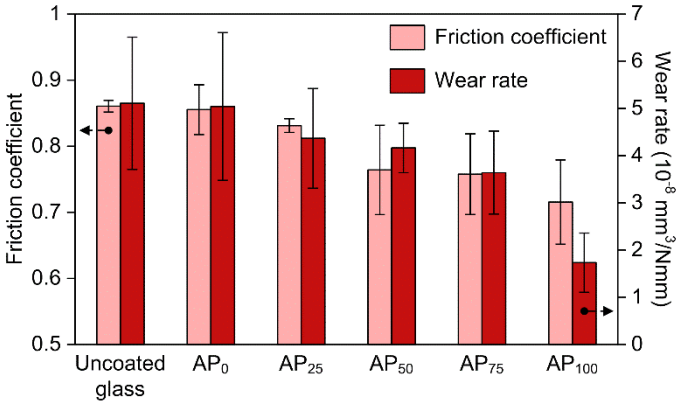
1
0.9
0.8
0.7
0.6
0.5
Friction coefficient
7
6
5
4
3
2
1
0
Wear rate (10-8 mm3/Nmm)
Friction coefficient
Wear rate
Uncoated glass
AP0
AP25
AP50
AP75
AP100

Fig. 10

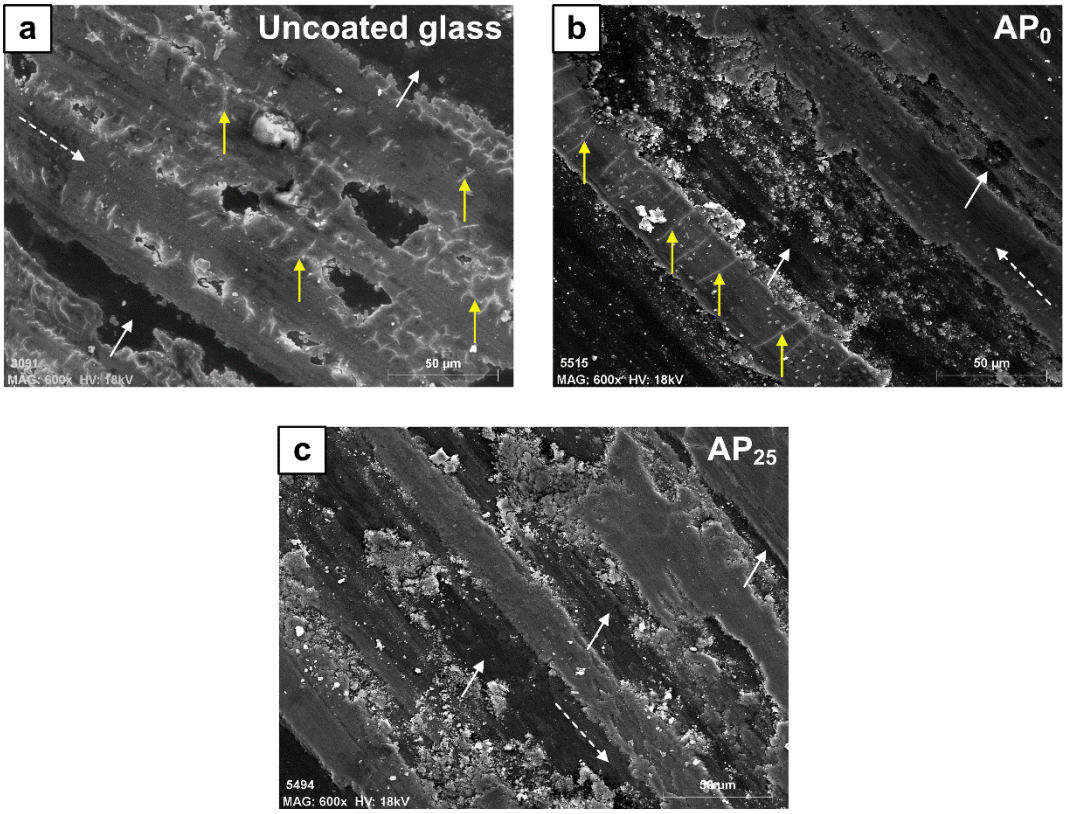
a
Uncoated glass
50 µm
b
AP0
5515
MAG: 600x HV: 18kV
50 µm
c
AP25
5494
MAG: 600x HV: 18kV

Fig. 11

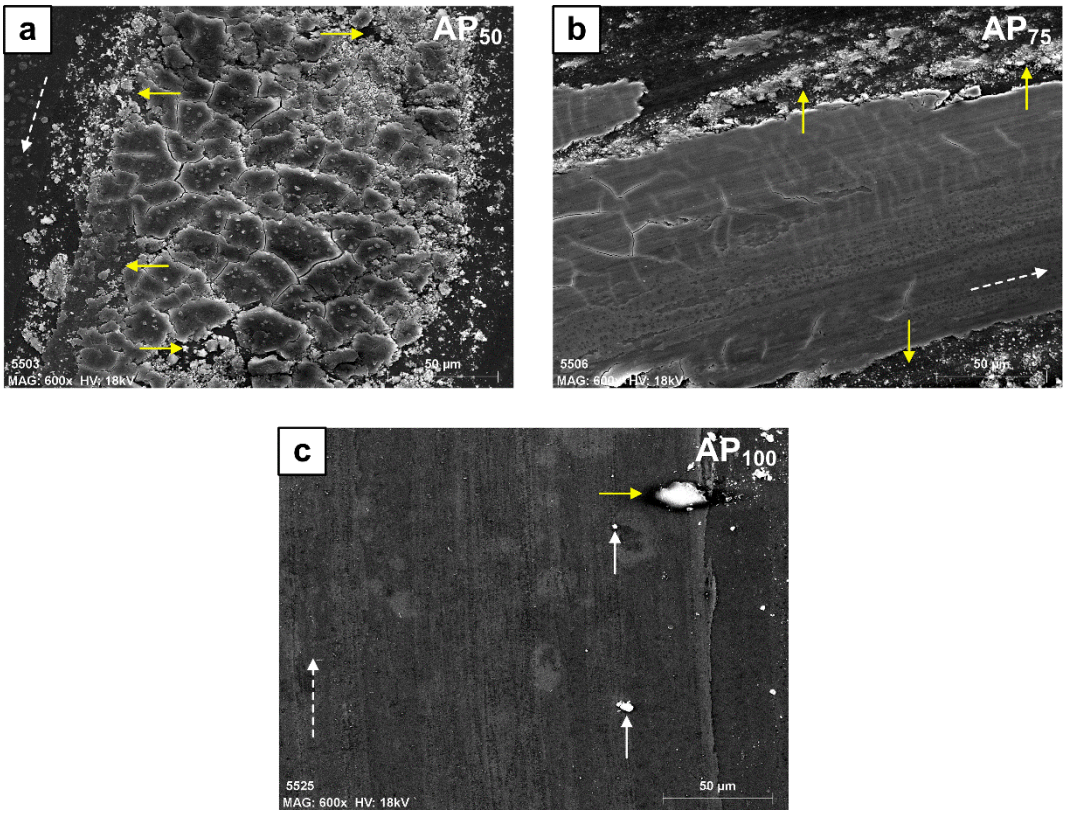
a
AP50
5503
MAG: 600x HV: 18kV
50 µm
b
AP75
5506
50 µm
c
AP100
5525
MAG: 600x HV: 18kV
50 µm

Fig. 12

Sample	Precursors (%)	
	APTES	PFH
AP_0	0	100
AP_{25}	25	75
AP_{50}	50	50
AP_{75}	75	25
AP_{100}	100	0
Uncoated glass	-	-

Table 1. Designation of the samples and their associated proportions of APTES and PFH.

Sample	Coating thickness (nm)	RMS roughness (nm)
AP_0	3.5 ± 2	15.4
AP_{25}	132.9 ± 4.7	195.6
AP_{50}	73.3 ± 7.7	174
AP_{75}	113.9 ± 7.7	181.3
AP_{100}	105.1 ± 3.5	14.2
Uncoated glass	-	4.9

Table 2. Coating thickness and RMS roughness of the studied samples.

Binding energy (eV)	Functional groups	References
~284.4	C-Si	[5]
~285	C-C, C-H	[5,16,19,27,33]
~286	C-N, C-CF	[1,19,33-35]
~286.5	C-O	[5,16,27]
~288	C=O, CF	[1,15,27,33,35]
~291.4	CF_2	[1,5,15,33]

Table 3. Functional groups and binding energies associated with the peaks considered in the deconvolution of the XPS spectra (C1s).